Theoretical Study of the First Acid Dissociation of H_2SO_4 at a Model Aqueous Surface†

Roberto Bianco,*,‡ Shuzhi Wang,‡ and James T. Hynes*,‡,§

Department of Chemistry and Biochemistry, University of Colorado, Boulder, Colorado 80309-0215, Département de Chimie, CNRS UMR 8640 PASTEUR, Ecole Normale Supérieure, 24 rue Lhomond, Paris 75231, France

Received: September 9, 2005; In Final Form: October 13, 2005

Electronic structure calculations on the $H_2SO_4 \cdot (H_2O)_{4,6}$ model system embedded at the surface of an aqueous layer have been performed to examine the feasibility of the first acid dissociation of H_2SO_4 to an $HSO_4^- \cdot H_3O^+$ contact ion pair over a wide temperature range, with a special focus on the 190−250 K range relevant for atmospheric sulfate aerosols. The results indicate that the acid dissociation can be either thermodynamically favored or disfavored depending on the degree of solvation of the acid and the produced ions, as well as on the temperature.

1. Introduction

Sulfuric acid (H_2SO_4) and its derived bisulfate (HSO_4^-) and sulfate (SO_4^{2-}) ionic species are present in various locations in the atmosphere in the form of sulfate aerosols (SAs), liquid supercooled aqueous solutions of sulfuric acid. The bulk composition of SAs is strongly dependent on the temperature and the water vapor pressure,[1,2] and thus varies in the polar stratosphere,[3−8] the midlatitude stratosphere (away from the poles),[2,9] and the Arctic boundary layer.[10−13] SAs can catalyze heterogeneous reactions important for ozone depletion[8] such as, the hydrolysis of N_2O_5 in the midlatitude stratosphere[2] and the reactions of $HOX + HBr \rightarrow BrX + H_2O$ (X = Br, Cl) in the Arctic boundary layer.[12,13] They can also influence the adsorption of strong acids such as HCl and HBr,[12,14,15] and oxidize organic species such as acetaldehyde (CH_3CHO).[16]

The catalytic properties of SAs for heterogeneous reactions are thought to derive from their high acidity and the presumed ability to assist reacting species by proton transfer (see, e.g., refs 9, 15, and 17) as well as by simple solvation. The understanding of such reactions would greatly benefit from a molecular level description of the surface region of SAs. However, while the bulk ionic composition of SAs is well described by thermodynamic models,[1] the ionic composition of the surface region is uncertain, despite a number of experimental investigations addressing this issue.[18,19] For example, under conditions where the SA bulk ionic composition is characterized by the complete first acid ionization of H_2SO_4

$$H_2SO_4 + H_2O \rightarrow HSO_4^- + H_3O^+ \qquad (1)$$

to produce the bisulfate and hydronium ions without any significant production of SO_4^{2-} ions via the second acid dissociation, it is not clear that the surface ionic composition is identical to that of the bulk. Thus, it is conceivable that molecular H_2SO_4 exists at the surface of such an SA due to the occurrence of the reverse of reaction 1 due to possibly reduced polarity conditions at the surface.

We are currently pursuing an approach based on the Reactive Monte Carlo methodology[20] to elucidate the structure of H_2SO_4 di- and tetrahydrate, both representative of high H_2SO_4 weight percentage SAs.[21] However, a molecular picture of the SA surface region is not yet available from these complex calculations. In the present paper, we follow an alternate approach, currently most suitable for dilute SAs, which has its origins in our methodology devised for the elucidation of reaction mechanisms for heterogeneous reactions on ice.[22,23] Thus, we are investigating the ability of H_2SO_4 to acid dissociate at the surface of an aqueous layer,[24] without the complications resulting from high H_2SO_4 concentrations.[1,24] Beyond providing an entree to the SA surface issue from the dilute H_2SO_4 regime, these investigations are also of interest in connection with studies related to ions at aqueous surfaces[25] and with studies of acid dissociation of H_2SO_4 in small water clusters.[26−28]

Our focus will be on the first acid dissociation (reaction 1) at an aqueous surface, and the question is whether this dissociation occurs. Given the widespread perception of H_2SO_4 as a "strong" acid, as well as the implied ease of its dissociation in small water clusters,[26−28] one might have difficulty entertaining the possibility that H_2SO_4 might not be dissociated in an aqueous environment. Beyond the issue of reduced polarity conditions at an interface noted above, it is relevant to note that the free energy of the first acid dissociation for H_2SO_4 in the bulk is estimated to be only approximately −3 kcal/mol[29] at 25 °C, with both enthalpic and entropic components likely to be strongly affected by the number of H-bonds formed by water molecules with, for example, the sulfate moiety of the acid (as well as by the temperature). In fact, our first effort on the acid dissociation reaction 1 at an aqueous surface[24] indicated that there may exist conditions at the surface of an aqueous layer rendering the H_2SO_4 dissociation endothermic at 0 K, albeit slightly, a possibility with obvious implications for the modalities in which acid catalysis of heterogeneous reactions may occur, i.e., with molecular H_2SO_4 rather than H_3O^+ acting as the proton donor. We extend this study by examining here further cases of acid dissociation of H_2SO_4 at the surface of an aqueous layer by keying on the degree of solvation of the sulfate

† Part of the special issue "Irwin Oppenheim Festschrift".

* Corresponding authors. E-mails: roberto.bianco@colorado.edu; hynes@spot.colorado.edu, hynes@chemie.ens.fr.

‡ University of Colorado.

§ Ecole Normale Supérieure.

10.1021/jp055107t CCC: $30.25
Published on Web 11/10/2005

TABLE 1: H_2SO_4 Calculated vs Experimental Structure

	exp[a]	HF[b]	MP2[c]
R(S═O)	1.422	1.414	1.429
R(S−OH)	1.574	1.573	1.602
R(O−H)	0.970	0.963	0.967
∠(O═S═O)	123.3	123.5	124.77
∠(O−S−O)	101.3	102.0	101.73
∠(O═S−O)	108.6	108.5	108.77
∠(O═S−O′)	106.4	106.2	105.27
∠(HOS)	108.5	109.9	107.66
∠(HOSO)		164.0	164.51

[a] Reference 61. [b] This work, HF/SBK+*. C_{2v} symmetry. In ∠(O═S−O) and ∠(O═S−O′), O is the oxygen H-bonded to the double bonded O, whereas O′ is the other, non H-bonded O. The ∠(HOSO) dihedral angle is calculated for the double bonded O non H-bonded to the OH. [c] MP2/6-311++G(2d,2p), ref 62.

group of the H_2SO_4 with implications for the solvation of the incipient HSO_4^- and H_3O^+ ions. In addition, we examine the acid dissociation over a range of temperatures, thus including thermal and entropic effects. We focus primarily on the temperature range 190−250 K, appropriate for SAs, with some discussion for temperatures outside this range, accessible to laboratory experiments. The relevant temperature range for SAs varies with location in the atmosphere. For example, in the midlatitude stratosphere, it is ∼210−240 K,[2] in the Antarctic stratosphere, it is ∼190−200 K,[7] while in the Arctic boundary layer, it is ∼230−250 K.[10]

The outline of the remainder of this paper is as follows. In section 2, we present our methodology and computational strategy. In section 3, we discuss our results for the energetics and free energetics of dissociation. Concluding remarks are offered in section 4.

2. Methodology

2.1. Electronic Structure Issues

2.1.1. Hartree-Fock Level of Theory. Our general methodology is described in detail in ref 24. Briefly, the $H_2SO_4{\cdot}(H_2O)_n{\cdot}W_m$, n/m = 4/13, 6/27, 4/26, model reaction system (MRS) comprises a $H_2SO_4{\cdot}(H_2O)_n$ core reaction system (CRS) embedded in a W_m cluster of classical, polarizable waters of fixed internal structure.[30] The CRS is treated quantum chemically at the HF/SBK+* level of theory, with the SBK[31] effective core potential basis set complemented by polarization (exp: S 0.65[32], O 0.8[33]) and diffused (exp: S 0.0405[34], O 0.0845[35]) functions. The W_m cluster provides both solvation and structural stability for the CRS, by preventing its collapse to structures non representative of a surface environment. GAMESS[36] was used for the calculations. The HF/SBK+* optimized structure of H_2SO_4 compares well with the experimental one and that obtained at the MP2/6-311+ +G(2d,2p) level of theory (cf. Table 1).

The W waters are parameterized to interact with a CRS described at the HF/DH(d,p) level of theory.[30] We have tested the SBK+* basis set vs DH(d,p) for the $H_2SO_4{\cdot}H_2O{\cdot}W$ cyclic complex, involving H-bonds typical of the larger clusters used here. The two structures are superimposed in Figure 1, where the orientation is such that the O of the H_2O H-bonded to the acidic proton is in the origin of the reference frame, the H_2SO_4 donor O is on the *z*-axis, pointing toward the top of the page, and the O of the length-marked S═O double bond lies in the plane of the page. The two structures have a large overlap. The HF/DH(d,p) bond lengths (in parentheses) are consistently lower than the HF/SBK+* ones. The largest difference of 0.053 Å, <3%, is in the HOH···W H-bond, whereas the important W(H)···O═S H-bond shows a difference of only 0.001 Å. For the case of a W(H)···OH_2 water dimer (not shown), the H-bond length is 2.078 Å for HF/SBK+* and 2.076 Å for HF/DH(d,p). Thus, the HF/SBK+* method is a good substitute for HF/DH(d,p) when using water-effective fragment potentials (Ws).[30]

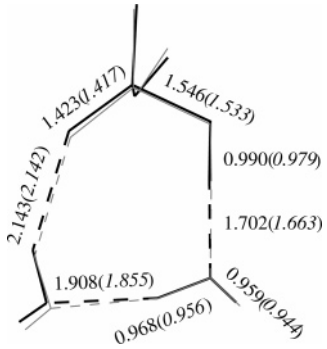

Figure 1. Structure comparison for $H_2SO_4{\cdot}H_2O{\cdot}W$ optimized at the HF/SBK+* (thick lines) and HF/DH(d,p) levels (thin lines). Clockwise from top: H_2SO_4, H_2O, and W. Bond distances in Å: SBK(*DH*). See text.

TABLE 2: Electronic Contributions[a] (PA_e) to the Proton Affinities of H_2O and HSO_4^-

	CBS	HF	MP2
$PA_e(H_2O)$	171.56[b]	169.11	165.87
$PA_e(HSO_4^-)$	318.58[c]	314.00	307.53
ΔPA_e	147.02	144.89	141.66

[a] HF:HF/SBK+*. MP2:MP2/SBK+*. All quantities in kcal/mol. For the gas-phase proton-transfer reaction $H_2SO_4 + H_2O \rightarrow HSO_4^- + H_3O^+$, $\Delta E_{rxn}(0\ K) = PA_e(HSO_4^-) - PA_e(H_2O)$, where PA_e is the electronic contribution to the proton affinity. [b] Reference 38. This is nearly identical to the CDSD(T)/aug-cc-pV5Z value[38] of 171.53 kcal/mol. The PA(298K) value[38] of 165.1 ± 0.3 kcal/mol at CBS level agrees well with the experimental value[39] of 165 kcal/mol. [c] Reference 40. The PA(0 K) and PA(298K) value[40] of 310.87 and 312.3 kcal/mol at CBS level are nearly identical with the G2 values[41] of 310.8 and 312.2 kcal/mol, respectively. The experimental values of PA(298K) are 309.6 ± 2.6[42] and 306.3 ± 3.1 kcal/mol,[43] respectively.

2.1.2. Estimates of Electron Correlation Effects. As discussed further within, the 0 K HF/SBK+* reaction free energy calculations for several of the cases examined, when augmented by zero point energy and thermal effects, give reaction free energies of the acid ionization that are small in magnitude, ∼0−3 kcal/mol either favorable or unfavorable. Such small magnitudes imply the need for an estimate of electron correlation effects in the 0 K reaction energies.

A first examination of these correlation effects compares, in Table 2, the electronic contributions (PA_e) to the gas-phase proton affinities (PA) of H_2O and HSO_4^- at the HF/SBK+* level and at the MP2/SBK+* level.[37] We will also later use the latter level in section 3 to estimate correlation effects for the H_2SO_4 ionization in various surface locations. Included for comparison is the PA_e result at a very high level of theory, CBS,[38] which, as indicated in the table, leads to very good agreement with experimental PAs. The HF/SBK+* value for the difference $PA_e(HSO_4^-) - PA_e(H_2O)$, which is the reaction energy $\Delta E_{rxn}(0\ K)$ for the $H_2SO_4 + H_2O \rightarrow HSO_4^- + H_3O^+$ gas phase reaction, is 2.13 kcal/mol less than the CBS level value 147.02 kcal/mol. This indicates a 2.13 kcal/mol bias in the HF/SBK+* calculations *in favor* of the proton transfer from H_2SO_4 to H_2O compared to the high level result. However, the MP2/SBK+* result shows an even larger bias of 5.36 kcal/mol in favor of the proton transfer. Thus, to correct for the

"intrinsic" deficiencies of the MP2/SBK+* estimates of electron correlation effects in the aqueous surface calculations of section 3, we must apply the correction factor +5.36 kcal/mol for the 0 K reaction energy.

Section 3 will detail the MP2/SBK+* level assessments of electron correlation effects carried out for the stable reactant and product complex structures found in the HF/SBK+* calculations for the several aqueous surface cases (cf. Table 3). These calculations, which are performed on a significant portion of the MRS for the various cases, indicate non-negligible electron correlation effects on the 0 K HF/SBK+* reaction energies. The latter are negative contributions, in the range 4−6 kcal/mol in magnitude, favoring the acid dissociation of H_2SO_4 by this amount more than the HF/SBK+* values. However, the considerations of the preceding paragraph indicate that these need to be corrected by +5.36 kcal/mol. The *net* effect is that the 0 K HF/SBK+* reaction energies for the H_2SO_4 acid dissociation are corrected by +0.96 to − 0.72 kcal/mol.

2.2. H_2SO_4 Placement and Reaction Paths. For the calculations within, using a classical lattice, the H_2SO_4 was initially placed atop or embedded within the surface layer of a W_{50} cluster with the structure of hexagonal ice,[44] and the MRS structure was partially relaxed via geometry optimization. This allows identification of the two Ws H-bonded to the two H_2SO_4 protons. Following this step, the MRS undergoes several cycles of visual inspections and reductions in the number of Ws, further partial optimizations, and enlargements of the CRS to its final size. This MRS, used for the reaction path calculations, has both protons on H_2SO_4 coordinated to quantum H_2Os, with the H_2O accepting the dissociating proton being further H-bonded to two other quantum H_2Os, able to stabilize the ensuing H_3O^+ ion.[45]

The initial search for the transition state (TS) region for the proton transfer (PT) was performed by mapping the MRS potential energy surface (PES) at fixed (and decreasing) $HO_3SOH\cdots OH_2$ H-bond distances, with all other MRS internal coordinates being optimized. When the region of the maximum for this one-dimensional path was identified, the PES mapping was expanded in that region as a function of the two $HO_3SO-H\cdots OH_2$ distances, and the saddle point region was located with greater accuracy. Finally, the TS was fully optimized.[46] With the fully characterized TS in hand, the intrinsic reaction coordinate path (IRC)[47] was obtained, and its end points were further optimized to the reactant complex (RC) and product complex (PC), and characterized by a frequency calculation.

2.3. Reaction Free Energetics. For the model systems used to investigate the H_2SO_4 dissociation in section 3, the reaction and activation free energies associated with the production of the $HSO_4^-\cdot H_3O^+$ contact ion pair (CIP) were calculated as $\Delta G,\Delta G^{\ddagger} = (E_{PC,TS} - E_{RC}) + (ZPE_{PC,TS} - ZPE_{RC}) + (H^{therm}_{PC,TS} - H^{therm}_{RC}) - T(S_{PC,TS} - S_{RC})$, where E is the energy at 0 K, ZPE is the zero point energy, H^{therm} is the thermal contribution from translational, rotational, and vibrational motions, and S is the entropy contribution from these motions. The thermal center of mass and overall rotational contributions, as well as a PV contribution to the enthalpy cancel in the differences on which we focus. Related definitions apply to changes in enthalpy and entropy.

For frequencies not assigned to sulfuric acid in the reactant complex and bisulfate ion in the product complex, the ZPEs and the vibrational contributions to the thermodynamic quantities were calculated using frequencies scaled by factors obtained via comparison between MP2/aug-cc-pVDZ[48] and HF/SBK+* calculated frequencies for the cyclic water tetramer. In particular, a mixed $(H_2O)_2\cdot W_2$ cyclic cluster, with alternate H_2O and W moieties around the ring, was used for the HF/SBK+* case, consistent with the larger model systems described in section 3. The $(H_2O)_2\cdot W_2$ vibrational modes were matched to those assigned in ref 48, as shown in Table 4. The MP2/aug-cc-pVDZ inter- and intramolecular frequencies fall, respectively, below and above 1000 cm^{-1}. The mode-specific comparison with HF/SBK+* frequencies in these two ranges[49] yields two average scaling factors, 1.0962 and 0.9173, for the inter- and intramolecular frequencies, respectively (not assigned to H_2SO_4 in the RC and HSO_4^- in the PC, see below), which have been used for the thermodynamic quantities in section 3.

Albeit obtained for a neutral water cluster, these scaling factors are also adequate for H_3O^+. A comparison between experimental[50,51] and HF/SBK+* frequencies for the H_3O^+ stretches in the $H_3O^+\cdot(H_2O)_3$ cluster (cf. Table 5), yielded an average scaling factor of 0.9067 for the H_3O^+ modes, suf-

TABLE 3: Electron Correlation Effects[a]

$H_2SO_4.(H_2O)_n$	ΔE(HF)	ΔE(MP2)
on-top, $n = 10$	6.52	0.44
semi-emb, $n = 10$	8.06	2.52
emb, surface OH, $n = 12$	7.43	3.03
emb, bulk OH, $n = 12$	−1.24	−5.70

[a] HF/SBK+* and MP2/SBK+* values are on sub-MRS excised from the corresponding, optimized MRS and larger than the CRS, with all waters treated quantum chemically. ΔE = E(PC) − E(RC). All values in kcal/mol.

TABLE 4: H_2O Tetramer Vibrational Frequencies (cm^{-1})

$(H_2O)^4$ [a]	$(H_2O)_2\cdot W_2$ [b]	s.f.[c]
	Intermolecular	
51	58.89	0.8660
79	76.47	1.0331
200	168.21	1.1890
211	181.77	1.1608
237	185.59	1.2770
237	194.56	1.2181
255	213.11	1.1966
255	258.62	0.9860
261	266.47	0.9795
291	309.03	0.9417
403	364.85	1.1046
435	375.25	1.1592
451	428.97	1.0514
451	432.86	1.0419
754	690.52	1.0919
826	698.33	1.1828
826	722.16	1.1438
996	898.51	1.1085
	Intramolecular	
1653	1801.01	0.9178
1683	1810.42	0.9296
3484	3945.50	0.8830
3522	3973.50	0.8864
3886	4117.38	0.9438
3887	4121.44	0.9431

[a] MP2/aug-cc-pVDZ frequencies from ref 48. [b] This work. Unscaled HF/SBK+* frequencies. [c] Mode-specific scaling factor. Average scaling factors: 1.0962 for intermolecular modes, and 0.9173 for intramolecular modes.

TABLE 5: $H_3O^+\cdot(H_2O)_3$ Vibrational Frequencies (cm^{-1})

exp[a]	HF[b]	s.f.[c]	mode
3730.4	4118.34	0.9058	in-phase asym str
3644.9	4016.32	0.9075	out-of-phase sym str

[a] Experimental frequencies from refs 50 and 51. [b] This work. Unscaled HF/SBK+* frequencies. [c] Mode-specific scaling factor. Average scaling factor: 0.9067.

TABLE 6: H_2SO_4 Vibrational Frequencies (cm^{-1})

		Ar[a]	HF[b]	s.f.[c]	mode[d]
A	ν_1	3563	4017.14	0.887	H−O s st
	ν_2	1216	1309.35	0.929	O═S═O s st
	ν_3	1136	1279.71	0.888	HOS s bnd
	ν_4	831	938.83	0.885	HO−S−OH s st
	ν_5	548	601.61	0.911	O═S═O bnd
	ν_6	422	489.83	0.862	twist at S
	ν_7	379	416.50	0.910	HO−S−OH bnd
	ν_8	224	306.42	0.731	HOSO s tor
B	ν_9	3567	4012.53	0.889	H−O as st
	ν_{10}	1452	1559.80	0.931	O═S═O as st
	ν_{11}	1157	1290.75	0.896	HOS as bnd
	ν_{12}	882	992.91	0.888	HO−S−OH as st
	ν_{13}	558	612.36	0.911	O═S═O wag
	ν_{14}	506	544.26	0.930	HO−S−OH wag
	ν_{15}	288	367.73	0.783	HOSO as tor

[a] Experimental Ar matrix vibrational frequencies from ref 62. [b] This work. Unscaled HF/SBK+* frequencies. [c] Mode-specific scaling factor. Average scaling factor: 0.882. [d] Mode description. Legend: st = stretch, bnd = bend, tor = torsion, wag = wagging, s = symmetric, as = asymmetric.

ficiently close to the 0.9173 factor adopted for the thermochemical calculations.

For H_2SO_4, a mode-by-mode comparison between experimental and HF/SBK+* frequencies (cf. Table 6), yields the average scaling factor 0.882, applied to both H_2SO_4 and HSO_4^- frequencies as assigned by visual inspection (using Molden[52]) of the RC and PC frequency sets for the system examined. This factor has been employed for the ZPEs and vibrational contributions in section 3.

3. Dissociation of H_2SO_4 at an Aqueous Layer

We have examined several cases with differing positions of the H_2SO_4 molecule at the surface, which thus have varying degrees of solvation for the sulfate moiety of the acid and of the proton-accepting water molecule.

3.1. H_2SO_4 Adsorbed on Top: $H_2SO_4\cdot(H_2O)_4\cdot W_{13}$. The first situation we modeled − which, as discussed below, is largely for perspective − involves H_2SO_4 adsorbed on top of a $(H_2O)_4\cdot W_{13}$ water layer, with the H_2O quantum and the W classical waters, with both acidic protons of H_2SO_4 H-bonded to H_2Os and with a single H-bond from a W to one of the double-bonded oxygens of H_2SO_4; this latter feature would stabilize the HSO_4^- anion produced in the first acid dissociation. The reactant complex for this MRS is depicted in Figure 2. Note that in the CRS, also shown in Figure 2, one of the acceptor H_2Os is H-bonded to two other H_2Os, to stabilize the ensuing H_3O^+ resulting from dissociation. We have explored the dissociation path by increasing stepwise the HO_3SO-H distance, starting at the RC and optimizing the remaining internal coordinates until the H-bond distance to the acceptor water was small enough to perform a constrained optimization of the PC/CIP with the H-bond distance to the acceptor water fixed at 1 Å to, essentially, force the formation of the $H_3O^+\cdot HSO_4^-$ contact ion pair. This process is strongly endothermic, with an energy increase (at 0 K) from the RC to this artificial PC of ΔE(HF) ∼ 9 kcal/mol. The unconstrained optimization of the artificial PC structure produced its relaxation to the original RC structure, thus confirming the endothermicity of the reaction and indicating the absence of a transition state.[54]

To assess electronic correlation/basis set effects for this case, as discussed in general terms in section 2.1.2, we have employed a sub-MRS system comprising the CRS with its first hydration layer, $H_2SO_4\cdot(H_2O)_{10}$, now with all waters treated quantum chemically, to perform MP2/SBK+* calculations. First, single point HF/SBK+* calculations on this system have been performed for the reactant and product complexes at their HF/SBK+* geometries for the $H_2SO_4\cdot(H_2O)_4\cdot W_{13}$ system calculated above. These give a 0 K reaction energy of +6.52 kcal/mol. Single point MP2/SBK+* calculations for $H_2SO_4\cdot(H_2O)_{10}$ using these same geometries give the 0 K reaction energy as 0.44 kcal/mol, providing a correction of −6.08 kcal/mol (cf. Table 3). Finally, to this is added the correction +5.36 kcal/mol derived from the intrinsic reaction energy correction in Table 2 from proton affinity considerations, to give a final electron correlation/basis set correction of −0.72 kcal/mol. Thus, the final estimate of the 0 K reaction energy ΔE for the on-top case is $\Delta E = \Delta E$(HF) − 0.72 kcal/mol ≃ 8 kcal/mol, again indicating the strongly endothermic character of the H_2SO_4 acid dissociation. As will become evident in the discussion of the further cases below, zero point energy and thermal effects will not change this basic conclusion.

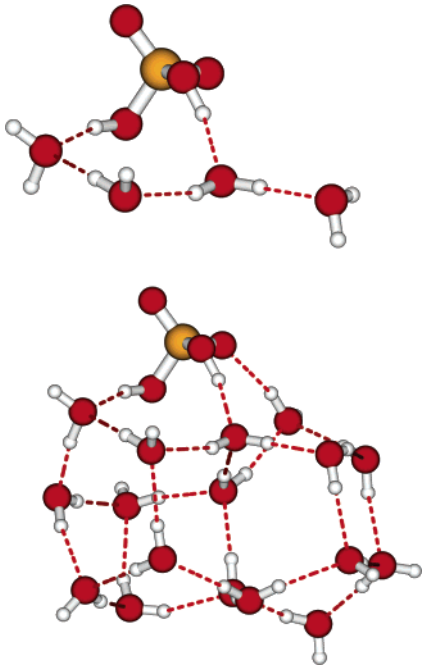

Figure 2. H_2SO_4 on top of a water layer. $H_2SO_4\cdot(H_2O)_4$ CRS (top) and $H_2SO_4\cdot(H_2O)_4\cdot W_{13}$ MRS. The reactant complex is shown.

Before proceeding to other arrangements of H_2SO_4 at the surface, we pause to place the above result in some perspective. The failure of sulfuric acid to dissociate in these conditions can be compared with the finding[23] that the stronger acid HCl fails to ionize atop an aqueous surface, even with the further direct solvation, beyond that by the H_3O^+ ion, by a single water of the incipient anion; the even stronger acid HBr is, however, found to ionize in such a situation.[23] Solvation of the Cl moiety of HCl by two waters can lead to acid ionization atop an aqueous surface.[23,55] In the arrangement Figure 2, the bisulfate moiety has only one water directly solvating a doubly bonded, negatively charged, oxygen. In the cases examined below, additional solvation of the sulfate moiety of H_2SO_4 will be present due to the embedding of the molecule in the surface region, and can be expected to assist the acid ionization.

3.2. H_2SO_4 Semi-Embedded: $H_2SO_4\cdot(H_2O)_6\cdot W_{27}$ → $HSO_4^-\cdot H_3O^+\cdot(H_2O)_5\cdot W_{27}$. In Figure 3 we show the MRS and the CRS for the dissociation of one of two H_2SO_4 protons located in the top surface layer (no bulk protons) in a positioning of the H_2SO_4 at the aqueous surface that we have already discussed in ref 24 (which we term semi-embedded "surface"

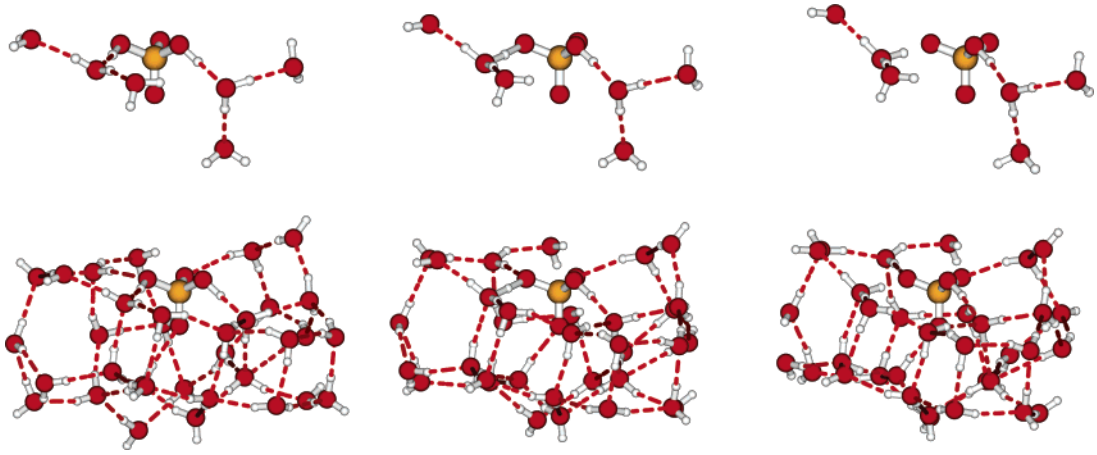

Figure 3. Reaction path highlights for the dissociation of one of the surface protons for a semi-embedded case. Reactant complex (left), transition state (middle), and product complex (right). CRS (top) and MRS. See Supporting Information, Coordinates File.

TABLE 7: Energetics and Thermodynamics of H_2SO_4 Dissociation at Model Water Layers[a]

T	30	60	90	120	150	180	210	240	270	300
				$H_2SO_4\cdot(H_2O)_6\cdot W_{27} \rightarrow HSO_4^-\cdot H_3O^+\cdot(H_2O)_5\cdot W_{27}$						
				(semi-embedded, surface proton dissociation)						
ΔG	3.44	3.42	3.43	3.43	3.44	3.44	3.48	3.49	3.53	3.56
ΔH	3.44	3.43	3.43	3.41	3.38	3.34	3.32	3.28	3.26	3.23
ΔS	0.08	0.09	−0.02	−0.20	−0.40	−0.58	−0.75	−0.89	−1.01	−1.10
				$\Delta E(\mathrm{HF}) = 2.76$; $\Delta E = 2.58$; $\Delta E + \Delta\mathrm{ZPE} = 3.44$						
				$H_2SO_4\cdot(H_2O)_4\cdot W_{26} \rightarrow HSO_4^-\cdot H_3O^+\cdot(H_2O)_3\cdot W_{26}$						
				(embedded, surface proton dissociation)						
ΔG	−0.26	−0.12	0.06	0.29	0.55	0.82	1.12	1.43	1.75	2.09
ΔH	−0.36	−0.47	−0.57	−0.67	−0.77	−0.90	−1.01	−1.13	−1.24	−1.35
ΔS	−3.24	−5.76	−7.03	−7.99	−8.81	−9.52	−10.12	−10.64	−11.08	−11.47
				$\Delta E(\mathrm{HF}) = -4.76$; $\Delta E = -3.80$; $\Delta E + \Delta\mathrm{ZPE} = -0.31$						
				$H_2SO_4\cdot(H_2O)_4\cdot W_{26} \rightarrow HSO_4^-\cdot H_3O^+\cdot(H_2O)_3\cdot W_{26}$						
				(embedded, bulk proton dissociation)						
ΔG	−1.47	−1.25	−0.99	−0.69	−0.39	−0.07	0.25	0.63	1.01	1.39
ΔH	−1.63	−1.74	−1.83	−1.90	−1.98	−2.07	−2.15	−2.26	−2.36	−2.47
ΔS	−5.33	−8.17	−9.34	−10.04	−10.60	−11.10	−11.58	−12.03	−12.45	−12.84
				$\Delta E(\mathrm{HF}) = -5.97$; $\Delta E = -5.07$; $\Delta E + \Delta\mathrm{ZPE} = -1.53$						

[a] T in K. Energy ΔE, free energy ΔG, enthalpy ΔH, and ZPEs in kcal/mol. Entropy ΔS in cal mol^{-1} K^{-1}. Thermal contributions calculated using the scaled frequencies discussed in section 2.3. The results for ΔG and ΔH if ΔE(HF) were used instead of ΔE can be obtained by adding the quantity $\Delta E(\mathrm{HF}) - \Delta E$.

proton dissociation). In that study, only 0 K results were reported. We supplement those here with free energy and thermal calculation results to compare with the H_2SO_4 dissociation results in the succeeding subsections.

The MRSs for this cluster, which is larger than the other MRS in the present work, has both H_2SO_4 protons solvated by a quantum water, which is in turn H-bonded to two other quantum waters. As noted in ref 24, and as discussed further in section 3.3, this arrangement can be regarded as a minimum solvation situation beyond the atop case presented in section 3.1. While it allows the dissociation of either acidic proton, only one will dissociate due to the weakly acidic character of the HSO_4^- ion, and the solvation of the ensuing hydronium ion by two quantum H_2Os is necessary, due to the inadequacy of W-waters in solvating H_3O^+. The HF/SBK+* energies at 0 K and the zero point energies for the RC, TS, and PC are $E_{RC}(\mathrm{HF}) = -175.413385$ h, $E_{TS}(\mathrm{HF}) = -175.408292$ h, $E_{PC}(\mathrm{HF}) = -175.408987$ h, such that $\Delta E(\mathrm{HF}) = 2.76$ kcal/mol, while $\mathrm{ZPE}_{RC} = 211.45$ kcal/mol, $\mathrm{ZPE}_{TS} = 210.14$ kcal/mol, and $\mathrm{ZPE}_{PC} = 212.31$ kcal/mol. Before proceeding, we determine the electron correlation/basis set correction to the ΔE(HF) value above via the same procedure as in section 3.2. Single point HF/SBK+* and MP2/SBK+* calculations for the sub-MRS system $H_2SO_4\cdot(H_2O)_{10}$, consisting of the CRS plus its first hydration layer for the present case, were performed for the HF/SBK+* reactant and product complexes determined above. These give the MP2/SBK+* − HF/SBK+* 0 K energy difference = (2.52 − 8.06) = −5.54 kcal/mol correction to ΔE(HF) (cf. Table 3). When the reaction energy correction +5.36 kcal/mol arising from proton affinity considerations in Table 2 is added to this, the final 0 K reaction energy $\Delta E = \Delta E(\mathrm{HF}) - 0.18$ kcal/mol is obtained. It is this ΔE value that is displayed and employed in the results collected in Table 7.

As already reported in ref 24, the dissociation is endothermic at 0 K, $\Delta E + \Delta\mathrm{ZPE} = 3.44$ kcal/mol, with the ΔZPE contributing only ∼0.9 kcal/mol. The reaction free energy ΔG in Table 7 is remarkably close to this over the entire temperature range reported, differing by only ∼0.1 kcal/mol; both the entropy contribution $-T\Delta S$ and the thermal contribution to ΔH are small, and tend to compensate each other, preserving the 0 K result both qualitatively and quantitatively. As we will see in the following subsections, there can be very important differences between ΔG and the 0 K energetics for other arrangements of H_2SO_4 at the aqueous surface. We have examined only the 0 K activation energy and free energies at the HF/SBK+* level for the MRS. At that level, the 0 K values of $\Delta E^{\ddagger}(\mathrm{HF})$ and $\Delta E^{\ddagger}(\mathrm{HF}) + \Delta\mathrm{ZPE}^{\ddagger}$ are 3.20 and 1.88 kcal/mol, respectively. The former is more than $\Delta E(\mathrm{HF}) = 2.76$ kcal/

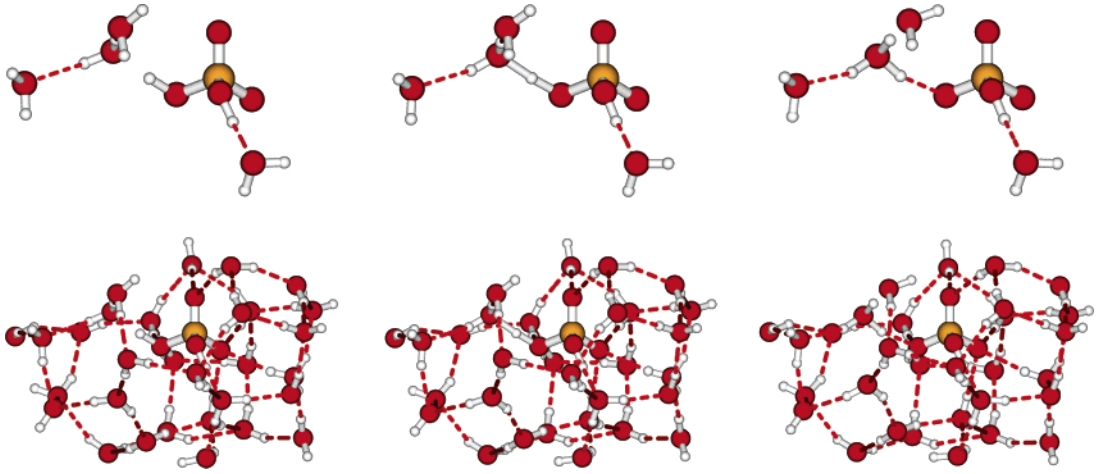

Figure 4. Reaction path highlights for the dissociation of the surface proton. Reactant complex (left), transition state (middle), and product complex (right). CRS (top) and MRS. See Supporting Information, Coordinates File.

mol, while the latter is less than ΔE(HF) + ΔZPE = 3.44 kcal/mol, indicating that the 0 K barrier at this level is obliterated by zero point energy effects, a situation not changed by thermal effects in the entire temperature range.

Details on the coordinates, zero point energies and entropies for the above case, as well as for the two further cases described below, are available as Supporting Information.

3.3. H_2SO_4 Fully Embedded: $H_2SO_4\cdot(H_2O)_4\cdot W_{26} \rightarrow HSO_4^-\cdot H_3O^+\cdot(H_2O)_3\cdot W_{26}$. The effect of further direct solvation on the sulfate group oxygens has been modeled by embedding the H_2SO_4 molecule deeper into the aqueous layer. We will contrast the dissociation of the acidic OH H-bonded to surface waters (which we term "surface" proton dissociation) with that of the acidic OH pointing toward the bulk (termed "bulk" proton dissociation). In each case, we have both acidic protons coordinated to quantum H_2Os, but we assist with two further quantum H_2Os the proton-accepting H_2O, leaving the other H_2Os solvated by classical Ws only, due to the high computational costs of the calculations. This situation is slightly different from that of section 3.2, where both acceptor H_2Os have a complement of two solvating H_2Os each. This is not an important limitation, however, since the first acid dissociation naturally hinders the dissociation of the other OH, which is left unconstrained throughout the calculations; sulfuric acid is a weak acid with respect to its second acid dissociation.

3.3.1. Surface Proton Dissociation. In Figure 4 we show the MRS for the dissociation of the surface proton, where the solvation of both doubly bonded Os of the sulfate moiety is displayed; the corresponding CRS is also shown in Figure 4. The further embedding of the H_2SO_4 leads to greater solvation of the HSO_4^- anion, whose H group points into the bulk, than for the case discussed in section 3.2. The energies at 0 K and the zero point energies for the RC, TS, and PC are: E_{RC}(HF) = −141.659226 h, E_{TS}(HF) = −141.658946 h, E_{PC}(HF) = −141.666809 h; ZPE_{RC} = 172.12 kcal/mol, ZPE_{TS} = 171.60 kcal/mol, ZPE_{PC} = 175.61 kcal/mol. The 0 K reaction energy is thus ΔE(HF) = −4.76 kcal/mol. The energetics and free energetics for the dissociation of the surface proton are summarized in Table 7.

Again, we assess electron correlation/basis set corrections to this ΔE(HF) value in the same fashion as in sections 3.1 and 3.2, based on single-point calculations for the sub-MRS system $H_2SO_4\cdot(H_2O)_{12}$ consisting of the CRS and its first hydration layer for the present case, at the reactant and product complex geometries determined in the HF/SBK+* calculated geometries for the MRS. The MP2/SBK+* − HF/SBK+* 0 K energy difference = (3.03−7.43) = −4.40 kcal/mol correction to ΔE(HF) (cf. Table 3). With the addition to this of the reaction energy correction +5.36 kcal/mol arising from proton affinity considerations in Table 2, the final 0 K reaction energy ΔE = ΔE(HF) + 0.96 kcal/mol = −3.80 kcal/mol. This ΔE value is displayed and employed in the results in Table 7 for the reaction energetics and free energetics.

The first point of interest in Table 7 for the surface proton dissociation case is that the acid ionization is in fact slightly exothermic at 0 K: ΔE + ΔZPE = −0.31 kcal/mol. The ZPE effects are important here; they reduce the magnitude of the ΔE exothermicity by ∼3.5 kcal/mol (as compared to ∼0.9 kcal/mol for the case of section 3.2). This marked excess of ZPE, and thus the vibrational frequencies in the system, for the product complex compared to the reactant complex, is dominated by the contribution (∼2.7 kcal/mol) from the frequency region below 1000 cm^{-1}, with a much smaller contribution (approximately +0.8 kcal/mol) from the mode frequencies above 1000 cm^{-1} (Supporting Information, Figure 2S and Table 2S). Again, we have examined the 0 K activation energy only at the HF/SBK+* level for the MRS, finding that $\Delta E^{\ddagger}$(HF) and $\Delta E^{\ddagger}$ + $\Delta ZPE^{\ddagger}$ are 0.18 and −0.34 kcal/mol respectively, so that the very small barrier is wiped out by the ZPE effects, a conclusion which is not changed by thermal effects.

The 0 K exothermicity (−0.31 kcal/mol) is sufficiently small that it is imperative to examine the thermal effects, including the entropy effects, on the proton transfer in free energy calculations, whose results are also shown in Table 7. At very low temperatures less than ∼70 K, ΔG is negative and the reaction is spontaneous. However, in the temperature range 190−250 K relevant for SAs, the first acid dissociation of H_2SO_4 is not thermodynamically spontaneous, although ΔG is rather small in magnitude, ∼1 kcal/mol. The reaction is actually exothermic throughout this temperature range, with $\Delta H \sim -1$ kcal/mol. Thus, the unfavorable entropic contribution $-T\Delta S$ is the most important in these positive ΔG values, with the negative ΔS values expected as a consequence of, e.g., orientational restrictions of water molecules by the ions in the ion pair product.

The decrease in entropy in the acid dissociation, which is completely dominated by the contribution from mode frequencies less than 1000 cm^{-1} (Supporting Information, Figure 5S and Table 2S), can be qualitatively connected to strengthened

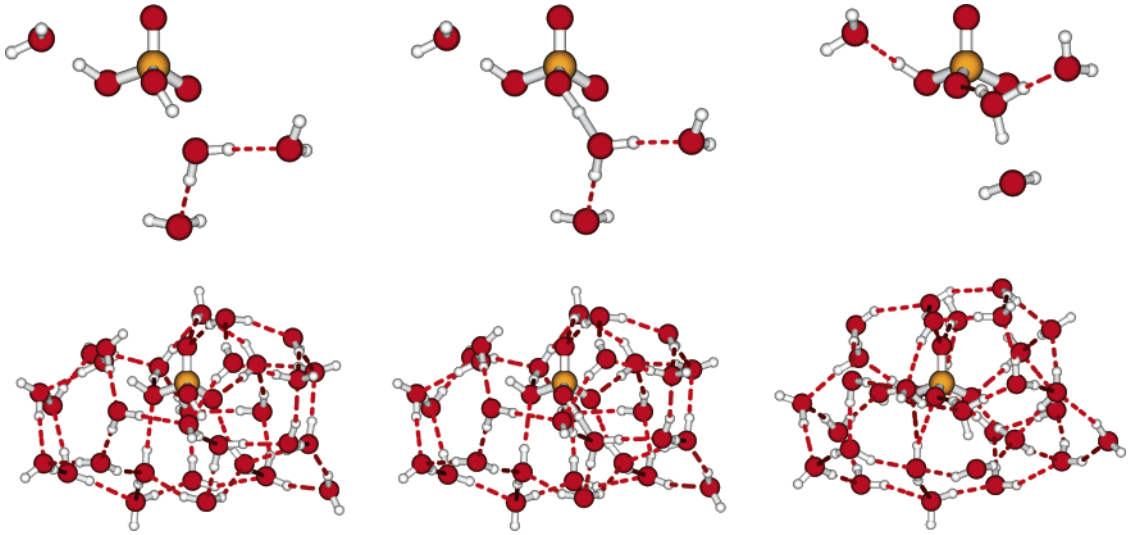

Figure 5. Reaction path highlights for the dissociation of the bulk proton. Reactant complex (left), transition state (middle), and product complex (right). CRS (top) and MRS. See Supporting Information, Coordinates File.

hydrogen bonds by inspection of the charges and bond distances in the PC and RC (Supporting Information, Figure 8S and Table 5S). In the contact ion pair PC, the charges on the oxygens of the sulfate moiety are more negative than in the RC, especially for the O that has donated the proton to a nearby water (from −0.76 to −0.87 e). Accordingly, the hydrogen bonds to nearby waters, and to the hydronium ion, are shortened (all this might be very loosely termed an "electrostriction effect"[56]).

3.3.2. Bulk Proton Dissociation. In Figure 5 we display the whole MRS for the dissociation of the bulk proton, where the H-bonding of waters to both of the sulfate moiety oxygens is evident; the CRS is also displayed in this figure. The energetics and free energetics for the dissociation of the bulk proton are reported in Table 7. The energies at 0 K and the zero point energies for the RC, TS, and PC are: E_{RC}(HF) = −141.667961 h, E_{TS}(HF) = −141.667568 h, E_{PC}(HF) = −141.677469 h; ZPE_{RC} = 173.57 kcal/mol, ZPE_{TS} = 173.04 kcal/mol, ZPE_{PC} = 177.11 kcal/mol. The 0 K HF/SBK+* reaction energy is thus ΔE(HF) = −5.97 kcal/mol.

Again, we estimate the correction to ΔE(HF) due to electron correlation/basis set effects based on single-point calculations for the sub-MRS system $H_2SO_4 \cdot (H_2O)_{12}$ consisting of the CRS and its first hydration layer for the present case, at the reactant and product complex geometries determined in the HF/SBK+* calculated geometries for the MRS. The MP2/SBK+* − HF/SBK+* 0 K energy difference = −5.70 − (−1.24) = −4.46 kcal/mol correction to ΔE(HF) (cf. Table 3). When the reaction energy correction +5.36 kcal/mol arising from proton affinity considerations in Table 2 is added to this, the final 0 K reaction energy $\Delta E = \Delta E$(HF) + 0.90 kcal/mol = −5.07 kcal/mol. This ΔE value is displayed and employed in the results in Table 7 for the reaction energetics and free energetics.

Table 7 shows that the 0 K energetics are again favorable for the dissociation: $\Delta E + \Delta ZPE$ = −1.53 kcal/mol, a value reduced in magnitude from the more favorable bare energetics ΔE by ∼3.5 kcal/mol by ZPE effects. In contrast to the surface proton dissociation case in section 3.3.1, the difference between the PC and RC ZPEs is dominated by mode frequencies above 1000 cm^{-1} (Supporting Information, Figure 3S and Table 3S). Again, the enhanced ZPE of the product complex compared to that for the reactant complex should be related to entropic effects for the reaction, discussed below.

In contrast to the surface proton dissociation case, the reaction is thermodynamically favored, with $\Delta G < 0$, up to ∼190 K, although ΔG is only of the order of −1 kcal/mol or less above ∼90 K. In the temperature range 190−250 K, the acid dissociation is not favored, although ΔG is less than 1 kcal/mol in magnitude. The reaction is exothermic at all temperatures examined, with the ΔH values approximately −2 kcal/mol above 120 K, but the unfavorable entropy effects ($-T\Delta S$), which are dominated by frequencies below 1000 cm^{-1} (Supporting Information, Figure 6S and Table 3S), significantly reduce the magnitude of ΔG compared to this, resulting in the slightly positive ΔG value above ∼200 K.

As was the case for the surface proton dissociation, the calculated PC and RC charges and bond distances (Supporting Information, Figure 9S and Table 6S) show that the entropy decrease in the acid ionization can be qualitatively correlated with increased hydrogen bonding in the ion pair product.

The remarks made for the previous two cases regarding the 0 K activation energy calculated at the HF/SBK+* level on the MRS apply here as well: $\Delta E^{\ddagger}$(HF) and $\Delta E^{\ddagger}$(HF) + $\Delta ZPE^{\ddagger}$ are 0.25 and −0.29 kcal/mol respectively, so that ZPE effects remove the small electronic barrier. This situation will not be changed by thermal effects.

4. Concluding Remarks

The calculated reaction free energies for the first acid dissociation of H_2SO_4 on/at model aqueous surfaces with varying degrees of solvation indicate that the feasibility of the dissociation is a quite sensitive function of the solvation and the temperature (Table 7).

For the first two cases considered, with H_2SO_4 atop and partially embedded in the surface layer, the reaction is endothermic at 0 K and remains thermodynamically unfavorable with a positive reaction free energy ΔG at finite temperatures up to 300 K, including the 190−250 K temperature range relevant for sulfate aerosols.

For two further cases examined with deeper embedding of the H_2SO_4 in the surface layer and with greater solvation of the sulfate moiety, the dissociation is favored energetically at 0 K, but the thermodynamic spontaneity of the reaction differs for the two cases. For the surface proton dissociation case (section 3.3.1), ΔG is negative only at temperatures below ∼70 K. In the sulfate aerosol temperature range, ΔG is ∼1 kcal/mol, and at 300 K, ΔG is ∼2 kcal/mol. For the bulk proton dissociation case (section 3.3.2), ΔG is negative over a wider range, up to

slightly below 190 K, and is positive over the sulfate aerosol range 190−250 K, although less than 1 kcal/mol in magnitude. Even at 300 K, ΔG is only ∼1 kcal/mol. Calculations with the H_2SO_4 even further embedded are underway to model the bulk situation itself to confirm that a ΔG value at ∼300 K of ∼−3 kcal/mol (see reaction 1) is obtained. The ΔG trends with temperature for these two cases indicate a greater ease of dissociation at lower temperatures, an aspect dominated by unfavorable entropy changes for the dissociation, a feature consistent with increased strength of hydrogen bonding in the ion pair products compared to the reactants. Some limited information is provided concerning any reaction barriers by the calculations. The small 0 K barriers in the bare energy (at the HF level) are obliterated by zero point energy effects, a situation not altered by thermal effects. Overall, these results suggest that while the acid ionization is favored at low temperatures, the situation is more delicate at higher temperatures. In particular, acid dissociation is not at all guaranteed at an aqueous surface layer in the higher portion of the temperature range 190−300 K, and that undissociated, molecular H_2SO_4 may exist at the surface. This issue could be addressed by surface-sensitive spectroscopy experiments,[19,57,58] and in a separate contribution[53] we provide detailed vibrational frequency information on the acid and its dissociation products to aid this end.

We pause to remark that this type of decrease in the thermodynamic driving force for acid dissociation with increasing temperature should also be taken into account for other acids, for example, HCl and HBr, as should the important role of the zero point energy. In addition, since nitric acid HNO_3 is evidently slightly weaker than H_2SO_4,[59] one can anticipate that a similar study of the acid ionization of HNO_3 at an aqueous surface, which is important in, for example, the stratosphere and the upper troposphere,[60] will indicate similar results, with acid ionization less likely.

We need to remark that several effects not included in the present calculations certainly require further investigation. The first is that the zero point energies and thermodynamic contributions to the reaction free energies have been calculated in the harmonic approximation for the vibrations calculated at 0 K geometries. At higher temperatures, particularly for the lower frequency vibrations, anharmonicities will become important and the hydration structures will change. It is difficult to assess the net importance of these effects except to note that, in a general way, one expects the solvation effects to diminish in magnitude with increasing temperature, which would imply that the H_2SO_4 acid ionization would become less favorable. The second, countervailing effect is that computational considerations have restricted the size of the systems we have been able to model. Addition of further waters would provide more solvation, favoring to some degree the acid dissociation. While these are likely not to be large given the size of the current systems (although we have not been able to reliably estimate them quantitatively), the small values of the reaction free energies for the various cases examined (e.g., less than a few kcal/mol in the final two entries of Table 7) indicate that they need not be negligible in impact. A possible method to explore the net consequences of the two effects discussed might be via Car−Parrinello simulations,[64] although the important impact of the zero point energies found within would also need to be taken into account.

Since the present results are for a single H_2SO_4 moiety, they are not directly applicable to the problem of the surface speciation of atmospheric aqueous sulfate aerosols relevant for ozone depletion, with H_2SO_4 concentrations in, for example, the 60−80 wt % range (i.e., approximately tetrahydrate to dihydrate). The delicate character of the dissociation found here suggests that further interactions present in the surface regions of such aerosols must be considered and may prove decisive. Among these are H_2SO_4−H_2SO_4 interactions as well as those of H_2SO_4 and the ionic reaction products with ionic species produced by acid dissociation in the bulk, which are in close proximity to the surface region, and indeed the ionic species located in the surface region itself arising from any acid dissociation occurring away from the site of the acid dissociation under consideration. For sulfate aerosols, these interactions may provide an effectively more polar surface region environment to better stabilize surface ionic species compared to the diluted environments examined here. As noted in the Introduction, this issue is under study via a Reactive Monte Carlo methodology.[20]

Finally, we have found that with sufficient solvation, i.e., for the embedded surface and bulk proton dissociation cases, the 0 K H_2SO_4 acid dissociation is exothermic. While in our studies the aqueous environment is much more extensive than those of small water cluster studies of this dissociation,[26] our results for these two cases are generally consistent with those studies, which find dissociation for, for example, four waters (on the other hand, for the on-top and semi-embedded cases in the present work, the acid ionization is found to be endothermic). However, even at 0 K, the present aqueous surface studies are obviously of a quite different character than those cluster studies and are not really comparable; in the cluster studies, the very few water molecules are free to rearrange to stabilize the contact ion pair without any of the important constraints of hydrogen-bonding to the remaining waters in the surface region and the bulk; constraints which evidently play a significant role in the present studies.

Acknowledgment. This work was supported in part by NSF grant ATM-0000542. This research was performed in part using the Molecular Science Computing Facility (MSCF) in the William R. Wiley Environmental Molecular Sciences Laboratory, a national scientific user facility sponsored by the U.S. Department of Energy's Office of Biological and Environmental Research and located at the Pacific Northwest National Laboratory. Pacific Northwest is operated for the Department of Energy by Battelle. J. T. Hynes expresses his appreciation for Irwin Oppenheim as both a scientist and a person.

Supporting Information Available: Structures of the RC, TS, and PC of CRS/MRS of semi-embedded surface proton dissociation, surface and bulk proton dissociation. Frequency distributions for ZPE of RC and PC and ΔZPE between RC and PC for the three cases. Frequency distributions for ΔS between RC and PC in the temperature range 30−300 K for the three cases. Changes of Mulliken charges and hydrogen bonding patterns from RC to TS and PC for the three cases together with figures. This material is available free of charge via the Internet at http://pubs.acs.org.

References and Notes

(1) Carslaw, K. S.; Peter, T.; Clegg, S. L. *Rev. Geophys.* **1997**, *35*, 125. Tabazadeh, A.; Toon, O. B.; Clegg, S. L.; Hamill, P. *Geophys. Res. Lett.* **1997**, *24*, 1931.

(2) Molina, M. J.; Molina, L. T.; Golden, D. M. *J. Phys. Chem.* **1996**, *100*, 12888.

(3) Fleming, E. L.; Chandra, S.; Barnett, J. J.; Corney, M. *Adv. Space Res.* **1990**, *10*, 1211.

(4) Ravishankara, A. R.; Hanson, D. R. *J. Geophys. Res. Atmos.* **1996**, *101*, 3885.

(5) Borrmann, S.; Solomon, S.; Dye, J. E.; Baumgardner, D.; Kelly, K. K.; Chan, K. R. *J. Geophys. Res. Atmos.* **1997**, *102*, 3639.

(6) Tolbert, M. A. *Science* **1994**, *264*, 527. Tolbert, M. A. *Science* **1996**, *272*, 1597.

(7) Solomon, S. *Rev. Geophys.* **1999**, *37*, 275.

(8) Seinfeld, J. H.; Pandis, S. N. *Chemistry and Physics: from Air Pollution to Climate Change*; Wiley-Interscience: New York, 1998.

(9) Robinson, G. N.; Worsnop, D. R.; Jayne, J. T.; Kolb, C. E.; Davidovits, P. *J. Geophys. Res. Atmos.* **1997**, *102*, 3583.

(10) Leaitch, W. R.; Hoff, R. M.; MacPherson, J. I. *J. Atmos. Chem.* **1989**, *9*, 187.

(11) Michalowski, B. A.; Francisco, J. S.; Li, S.-M.; Barrie, L. A.; Bottenheim, J. W.; Shepson, P. B. *J. Geophys. Res. Atmos.* **2000**, *105*, 15131.

(12) Abbatt, J. P. D.; Nowak, J. B. *J. Phys. Chem. A* **1997**, *101*, 2131.

(13) Fan, S.-M.; Jacob, D. J. *Nature* **1992**, *359*, 522.

(14) Morris, J. R.; Behr, P.; Antman, M. D.; Ringeisen, B. R.; Splan, J.; Nathanson, G. M. *J. Phys. Chem. A* **2000**, *104*, 6738.

(15) Waschewsky, G. C. G.; Abbatt, J. P. D. *J. Phys. Chem. A* **1999**, *103*, 5312.

(16) Duncan, J. L.; Schindler, L. R.; Roberts, J. T. *J. Phys. Chem. B* **1999**, *103*, 7247.

(17) Donaldson, D. J.; Ravishankara, A. R.; Hanson, D. R. *J. Phys. Chem. A* **1997**, *101*, 4717.

(18) Fairbrother, D. H.; Johnston, H.; Somorjai, G. *J. Phys. Chem.* **1996**, *100*, 13696.

(19) (a) Baldelli, S.; Schnitzer, C.; Shultz, M. J.; Campbell, D. J. *J. Phys. Chem. B* **1997**, *101*, 10435. (b) Schnitzer, C.; Baldelli, S.; Shultz, M. J. *Chem. Phys. Lett.* **1999**, *313*, 416. (c) Radüge, C.; Pflumio, V.; Shen, Y. R. *Chem. Phys. Lett.* **1997**, *274*, 140.

(20) Johnson, J. K. *Adv. Chem. Phys.* **1999**, *105*, 461.

(21) Bianco, R.; Wang, S.; Hynes, J. T., in progress.

(22) (a) Bianco, R.; Hynes, J. T. *J. Phys. Chem. A* **1999**, *103*, 3797. Bianco, R.; Hynes, J. T. *J. Phys. Chem. A* **1998**, *102*, 309. Bianco, R.; Hynes, J. T. *J. Phys. Chem. A* **2003**, *107*, 5253. (b) Bianco, R.; Hynes, J. T. *Acc. Chem. Res.*, in press.

(23) Al-Halabi, A.; Bianco, R.; Hynes, J. T. *J. Phys. Chem. A* **2002**, *106*, 7639.

(24) Bianco, R.; Hynes, J. T. *Theor. Chem. Acc.* **2004**, *111*, 182.

(25) Mucha, M.; Frigato, T.; Levering, L. M.; Allen, H. C.; Tobias, D. J.; Dang, L. X.; Jungwirth, P. *J. Phys. Chem. B* **2005**, *109*, 7617. A likely distribution of H_3O^+ and HSO_4^- ions at a liquid water interface is discussed here, although the H_2SO_4 acid dissociation is not examined.

(26) (a) Kurdi, L.; Kochanski, E. *Chem. Phys. Lett.* **1989**, *158*, 111. (b) Arstila, H.; Laasonen, K.; Laaksonen, A. *J. Chem. Phys.* **1998**, *108*, 1031. (c) Bandy, A. R.; Ianni, J. C. *J. Phys. Chem. A* **1998**, *102*, 6533. (d) Re, S.; Osamura, Y.; Morokuma, K. *J. Phys. Chem. A* **1999**, *103*, 3535. (e) Ding, C.-G.; Laasonen, K. *Chem. Phys. Lett.* **2004**, *390*, 307. (f) Natsheh, A. A.; Nadykto, A. B.; Mikkelsen, K. V.; Yu, F. Q.; Ruuskanen, J. *J. Phys. Chem. A* **2004**, *108*, 8914.

(27) (a) Ianni, J. C.; Bandy, A. R. *J. Mol. Struct. (Theochem)* **2000**, *497*, 19. (b) Ding, C.-G.; Laasonen, K.; Laaksonen, A. *J. Phys. Chem. A* **2003**, *107*, 8648.

(28) Large cluster studies involving classical, rather than quantum, interactions also exist: Kathmann, S. M.; Hale, B. N. *J. Phys. Chem. B* **2001**, *105*, 11719.

(29) Atkins, P.; de Paula, J. *Chemistry*, 7th ed.; Freeman: New York, 2002.

(30) Day, P. N.; Jensen, J. H.; Gordon, M. S.; Webb, S. P.; Stevens, W. J.; Krauss, M.; Garmer, D.; Basch, H.; Cohen, D. *J. Chem. Phys.* **1996**, *105*, 1968. Chen, W.; Gordon, M. S. *J. Chem. Phys.* **1996**, *105*, 11081.

(31) Stevens, W. J.; Basch, H.; Krauss, M. *J. Chem. Phys.* **1984**, *81*, 6026.

(32) Hariharan, P. C.; Pople, J. A. *Theor. Chem. Acc.* **1973**, *28*, 213.

(33) Pietro, W. J.; Francl, M. M.; Hehre, W. J.; DeFrees, D. J.; Pople, J. A.; Binkley, J. S. *J. Am. Chem.* Soc. **1982**, *104*, 5039.

(34) Spitznagel, G. W.; Diplomarbeit, Erlangen, 1982.

(35) Clark, T.; Chandrasekhar, J.; Spitznagel, G. W.; Schleyer, P. v. R. *J. Comput. Chem.* **1983**, *4*, 294.

(36) Schmidt, M. W.; Baldridge, K. K.; Boatz, J. A.; Elbert, S. T.; Gordon, M. S.; Jensen, J. H.; Koseki, S.; Matsunaga, N.; Nguyen, K. A.; Su, S. J.; Windus, T. L.; Dupuis, M.; Montgomery, J. A. *J. Comput. Chem.* **1993**, *14*, 1347. The URL for the GAMESS website is http://www.msg.ameslab.gov/GAMESS/GAMESS.html.

(37) Møller, C.; Plesset, M. S. *Phys. Rev.* **1934**, *46*, 618.

(38) Peterson, K. A.; Xantheas, S. S.; Dixon, D. A.; Dunning, T. H. *J. Phys. Chem. A* **1998**, *102*, 2449.

(39) Hunter, E. P.; Lias, S. G. *J. Phys. Chem. Ref. Data* **1998**, *27*, 413.

(40) Alexeev, Y.; Windus, T. L.; Zhan, C.-G.; Dixon, D. A. *Int. J. Quantum Chem.* **2005**, *102*, 775.

(41) Rustad, J. R.; Dixon, D. A.; Kubicki, J. D.; Felmy, A. R. *J. Phys. Chem. A* **2000**, *104*, 4051.

(42) Viggiano, A. A.; Henchman, M. J.; Dale, F.; Deakyne, C. A.; Paulson, J. F. *J. Am. Chem. Soc.* **1992**, *114*, 4229.

(43) Wang, X. B.; Nicholas, J. B.; Wang, L. S. *J. Phys. Chem. A* **2000**, *104*, 504.

(44) Hayward, J. A.; Reimers, J. R. *J. Chem. Phys.* **1997**, *106*, 1518.

(45) The H_2O EFP is not suitable for coordination to the H_3O^+ ion: the H-bonded proton from H_3O^+ promptly transfers to the H_2O EFP forming a bond of 0.5 Å.

(46) Due to the extremely soft MRS degrees of freedom, we set tighter thresholds for the integrals, energy, and gradients, namely: (i) INTTYP=HONDO, ITOL = 25, ICUT = 12 in the $CONTRL group; (ii) NCONV = 10 in the $SCF group; (iii) OPTTOL = 1E-6 in the $STATPT group. The calculation of the vibrational frequencies is also very delicate and required VIBSIZ = 0.005 with NVIB = 1.

(47) Ishida, K.; Morokuma, K.; Komornicki, A. *J. Chem. Phys.* **1977**, *66*, 2153 and references therein.

(48) Xantheas, S. S.; Dunning, T. H., Jr. *J. Chem. Phys.* **1993**, *99*, 8774.

(49) Since the EFPs have frozen internal structure, the intramolecular frequencies of the fragments are not calculated.

(50) Yeh, L. I.; Okumura, M.; Myers, J. D.; Price, J. M.; Lee, Y. T. *J. Chem. Phys.* **1989**, *91*, 7319.

(51) Yeh, L. I.; Lee, Y. T.; Hougen, J. T. *J. Mol. Spectrosc.* **1994**, *164*, 473.

(52) Schaftenaar, G.; Noordik, J. H. A pre- and postprocessing program for molecular and electronic structures *J. Comput.-Aided Mol. Design* **2000**, *14*, 123. Molden is available free of charge for academic use at http://www.cmbi.ru.nl/molden/molden.html.

(53) Bianco, R.; Wang, S.; Hynes, J. T., to be submitted.

(54) Since the artificial PC is not a local minimum, its zero point energy is not defined; this is the reason no zero point energy correction has been provided for the 0 K energy calculations in this section.

(55) (a) Svanberg, M.; Pettersson, J. B. C.; Bolton, K. *J. Phys. Chem. A* **2000**, *104*, 5787. (b) Devlin, J. P.; Uras, N.; Sadlej, J.; Buch, V. *Nature* **2002**, *417*, 269. (c) Bolton, K. *Int. J. Quantum Chem.* **2004**, *96*, 607. (d) Mantz, Y. A.; Geiger, F. M.; Molina, L. T.; Molina, M. J.; Trout, B. L. *Chem. Phys. Lett.* **2001**, *348*, 285. (e) For ionization of HCl at, rather than atop, an ice surface, see ref 63.

(56) Laidler, K. J. *Kinetics*, 3rd ed.; McGraw-Hill: New York, 1987.

(57) Morita, A.; Hynes, J. T. *J. Phys. Chem. B* **2002**, *106*, 673. Morita, A.; Hynes, J. T. *Chem. Phys.* **2000**, *258*, 371.

(58) Brown, E. C.; Mucha, M.; Jungwirth, P.; Tobias, D. J. *J. Phys. Chem. B* **2005**, *109*, 7934.

(59) Oxtoby, D. W.; Nachtrieb, N. H. *Principles of Modern Chemistry*, 2nd ed.; Saunders: Philadelphia, 1990.

(60) Zondlo, M. A.; Hudson, P. K.; Prenni, A. P.; Tolbert, M. A. *Annu. Rev. Phys. Chem.* **2000**, *51*, 473.

(61) Kuczkowski, R. L.; Suenram, R. D.; Lovas, F. J. *J. Am. Chem. Soc.* **1981**, *103*, 2561.

(62) Givan, A.; Larsen, L. A.; Loewenschuss, A.; Nielsen, C. J. *J. Mol. Struct.* **1999**, *509*, 35.

(63) Gertner, B. J.; Hynes, J. T. *Science* **1996**, *271*, 1563. Gertner, B. J.; Hynes, J. T. *Faraday Discuss.* **1998**, *110*, 301.

(64) Kuo, I. F. W.; Mundy, C. J.; McGrath, M. J.; Siepmann, J. I.; VandeVondele, J.; Sprik, M.; Hutter, J.; Chen, B.; Klein, M. L.; Mohamed, F.; Krack, M.; Parrinello, M. *J. Phys. Chem. B* **2004**, *108*, 12990.